DOI: 10.26599/FSHW.2025.9250860

Contents lists available at SciOpen

Food Science and Human Wellness

journal homepage: https://www.sciopen.com/journal/2097-0765

China Food Publishing Co.

Cyclocarya paliurus triterpenoids alleviate hyperuricemic nephropathy by regulating urate transporters and inhibiting the STAT3 signaling pathway

Rui Gui[a], Yi-Jin Xu[b], Zhi-Chun Yang[a,d], Jian-Ping Wu[a,d], Xiao-Qing Wang[a], Wen-Bo Yang[a], Qian Yao[a], Xi-Fan Wei[a], Zi-Yu Yan[a], Lu Bi[a], Yu-Fei Yang[a], Yi-Kun Wang[a,d], Wen-Xuan Wang[a,d], Qi Pei[c], Xia Yu[a,d*], Kang-Ping Xu[a,d*]

[a]*Xiangya School of Pharmaceutical Sciences, Central South University, Changsha 410013, PR China*

[b]*College of Horticulture, Hunan Agricultural University, Changsha, 410128, PR China*

[c]*The Third Xiangya Hospital, Central South University, Changsha, 410013, PR China*

[d]*Hunan Key laboratory of Diagnostic and Therapeutic Drug Research for Chronic Diseases, Changsha, 410013, PR China*

ABSTRACT: Hyperuricemic nephropathy (HN), characterized by renal inflammation and fibrosis, has an increased risk of progression to end-stage renal disease, with therapeutic drugs currently insufficient. This study aimed to investigate the effects and mechanisms of triterpenoids of *Cyclocarya paliurus* leaves (CPT) on HN *in vivo* and *in vitro*. The HN rat model was established through gavage of adenine (150 mg/kg) and ethambutol (250 mg/kg) over three weeks. Concurrently, CPT (150 mg/kg) was administrated orally. The levels of uric acid (UA), creatinine, and urea nitrogen in plasma and urine were measured. Hematoxylin-eosin and Masson's trichrome staining were performed on kidney tissues. The chemical composition of CPT was identified via HPLC-Q-TOF-MS/MS, and its targets for HN were screened through network pharmacology and molecular docking, cellular thermal shift assay (CETSA), surface plasmon resonance (SPR), and dual-luciferase reporter assay. Plasma metabolomics and renal proteomics were conducted to elucidate the mechanisms of CPT in mitigating HN. The renal expression of protein related to inflammation, fibrosis, and UA excretion in HN rats or UA-treated HK-2 cells was detected. CPT significantly reduced plasma UA levels and attenuated renal inflammation, fibrosis, and pathological alterations in HN rats. CPT promoted UA excretion and improved purine metabolism by downregulating the expressions of urate transporter 1 and glucose transporter 9 and upregulating the expression of organic anion transporter 1. Furthermore, CPT suppressed the inter interleukin-6 (IL-6)/signal transducer and activator of transcription 3 (STAT3)/suppressors of cytokine signaling 3 (SOCS3) signaling pathway, decreased epithelial-mesenchymal transition, and reduced the levels of presenilin-associated rhomboid-like protein and cysteine and glycine-rich protein 2 (CSRP2) in both HN rats and UA-stimulated HK-2 cells. CETSA and SPR showed that CPT and cypaliuruside B (a seco-triterpenoid isolated from CPT) directly bind to STAT3. Moreover, STAT3 directly binds to the CSRP2 promoter, enhancing its transcriptional activity. These results indicated that CPT alleviated HN by regulating renal UA transporters and inhibiting STAT3, which supports the potential application of CPT in treating hyperuricemia and related kidney diseases.

Keywords: *Cyclocarya paliurus*; triterpenoids; hyperuricemic nephropathy; STAT3; urate transporters.

***Corresponding author**
xyu226@csu.edu.cn (Xia Yu); xukp395@csu.edu.cn (Kang-Ping Xu)

Received 23 January 2025
Received in revised from 3 March 2025
Accepted 7 October 2025

1. Introduction

Hyperuricemia is characterized by abnormally elevated blood uric acid (UA) levels, primarily resulting from disorders in purine metabolism caused by either overproduction or reduced excretion of UA[1, 2]. Prolonged hyperuricemia not only leads to gout and kidney disease but is also closely associated with diabetes, hyperlipidemia, hypertension, and cardiovascular disease[3]. Hyperuricemia nephropathy (HN), also known as gouty nephropathy or UA nephropathy, refers to renal injury caused by hyperuricemia, characterized by renal inflammation, glomerular damage, and tubular interstitial fibrosis[4]. Hyperuricemia contributes to HN through mechanisms such as renal inflammation, epithelial-mesenchymal transition (EMT), oxidative stress, endothelial dysfunction, and activation of the renin-angiotensin system[5, 6]. The overall prevalence in China increased from 8.4% in 2009 to 14% in 2018, with higher rates observed in Europe, Africa, America, Japan, and Mexico[2, 7-9]. More than 15% of patients with hyperuricemia have stage 3 or more severe chronic kidney disease, which is significantly higher than 3% of the population with normal UA levels[10]. Furthermore, the risk of end-stage kidney disease in male and female patients with hyperuricemia is elevated by 4 times and 9 times, respectively[5]. However, there is still a lack of specific therapeutic drugs for HN[11]. Current UA-lowering medications are ineffective in controlling the progression of HN and can lead to many serious adverse reactions, including hypersensitivity reactions, gastrointestinal disturbances, and hepatorenal damage[12]. Therefore, it is essential to explore drugs that possess both hypouricemic and renoprotective effects to treat HN.

UA, the ultimate product of purine metabolism in humans, is primarily generated in the liver through various enzyme-catalyzed reactions and then excreted via the kidneys or intestines. Many urate transporters are distributed in renal tubules, including reabsorption transporters such as urate transporter 1 (URAT1) and glucose transporter 9 (GLUT9), as well as excretion transporters such as organic anion transporter 1 (OAT1), organic anion transporter 3 (OAT3), and ATP-binding cassette efflux transporter G2 (ABCG2)[3]. Hyperuricemia can lead to renal inflammation and oxidative stress through multiple mechanisms including the JAK/STAT3, TGF-β1/SMAD3, and PI3K/AKT pathways, thereby contributing to the development and progression of HN[11]. The signal transducer and activator of transcription 3 (STAT3) is a cytoplasmic transcription factor. It undergoes dimerization and subsequent nuclear translocation to modulate gene expression after its phosphorylation at tyrosine residue 705[13]. STAT3 is instrumental in the development of renal fibrosis and chronic kidney disease. The STAT3 inhibitor S3I-201 has been shown to significantly attenuate renal fibrosis in HN mouse models[13]. Furthermore, a range of natural products, including Fuling-Zexie formula, Simiao San, Qinling liquid, fucoidan, apigenin, fisetin, astilbin, and berberrubine, have demonstrated efficacy in ameliorating HN through inhibition of the STAT3 signaling pathway[14-21]. EMT significantly promotes HN, contributing to the augmented fibroblast population in renal fibrosis and leading to increased production of extracellular matrix components such as collagen I and fibronectin[17, 22].

Traditional Chinese medicine and natural products are a rich source for the discovery of new drugs for treating HN[4, 11]. *Cyclocarya paliurus* (Batal.) Iljinskaja, also known as “sweet tea tree”, a medicinal and

edible species endemic to China, belongs to the genus *Cyclocarya* within the *Juglandaceae* family[23, 24]. *C. paliurus* leaves contain multiple bioactive components like triterpenoids, flavonoids, and polysaccharides, which can be used to improve metabolic diseases[23]. Therefore, *C. paliurus* leaves are widely utilized as vegetables, tea beverages, and functional food additives, contributing to the alleviation of conditions such as diabetes, hyperlipidemia, and fatigue[23-26]. Recent research highlights that the aqueous extracts of *C. paliurus* leaves can effectively lower blood UA levels by inhibiting the activity of xanthine oxidase (XOD, a key enzyme in the production of UA) and regulating the expression of renal urate transporters. Meanwhile, these extracts mitigate kidney inflammation and fibrosis induced by hyperuricemia[27-29]. The triterpenoids are one of the characteristic active components found in *C. paliurus* leaves, which exhibit activities such as anti-cancer, anti-inflammatory, antioxidant, hypoglycemic, antibacterial, and lipid-regulating effects[30]. More than 160 triterpenoids have been isolated and identified from *C. paliurus*, which can be structurally divided into 3,4-seco-dammarane, dammarane, oleanane, and other types[23, 30, 31]. Recent studies indicate that the triterpenoids of *C. paliurus* leaves (CPT) improve renal damage, insulin resistance, and non-alcoholic fatty liver disease (NAFLD) by modulating the ROCK, AMPK/mTOR, TLR4/NF-kB/NLRP3, PI3K/Akt/GSK3β, or Rho-Kinase signaling pathways[32-36]. However, there are no reports on the effects and mechanisms of CPT on HN.

This research investigated the chemical composition of CPT utilizing HPLC-Q-TOF-MS/MS. Subsequently, the impact of CPT on HN was evaluated in both an HN rat model and HK-2 cells, which were induced by adenine combined with ethambutol and UA, respectively[6, 22]. The mechanisms by which CPT improves HN were explored through the integration of network pharmacology, plasma untargeted metabolomics, and renal label-free proteomics.

2. Materials and methods

2.1 Chemicals and materials

The urine protein detection kit was acquired from Nanjing Jiancheng Bioengineering Institute (Nanjing, China). Enzyme-linked immunosorbent assay (ELISA) kits to measure rat TNF-α, IL-6, and TGF-β1 were sourced from Cusabio Technology Co., Ltd (Wuhan, China). Primary antibodies including GLUT9 (67530-1-Ig), STAT3 (60199-1-Ig), SOCS3 (66797-1-Ig), E-cadherin (60335-1-Ig), Vimentin (60330-1-Ig), PARL (26679-1-AP), and CSRP2 (10892-2-AP) were obtained from Proteintech (Wuhan, China). Additionally, the IL-6 (NBP2-78132SS) antibody was procured from Novus Biologicals (Shanghai, China), the COL1A1 (E8I9Z) antibody from Cell Signaling Technology (Shanghai, China), and the p-STAT3 (ab76315) antibody from Abcam (Shanghai, China). Human STAT3 protein (HY-P701098), S3I-201 (HY-15146, a STAT3 inhibitor), and colivelin (HY-P1061, a STAT3 agonist) were purchased from MedChemExpress (Shanghai, China). The plasmids, such as STAT3-pc DNA-3.1 MYC, empty plasmid 3.1 MYC, pGL3-basic (containing the CSRP2 promoter sequence), and pRL-TK were procured from HanYi Biosciences Inc (Guangzhou, China). HK-2 cells were procured from Pricella (Wuhan, China), and fetal

bovine serum was supplied by VivaCell (Shanghai, China). Other reagents in this investigation conformed to those in the previous report [28].

2.2 CPT preparation and composition analysis

CPT was prepared as described in our preceding study[28]. The constituent analysis of CPT was conducted using HPLC-Q-TOF-MS/MS. The HPLC-MS system comprised 1290 Infinity II liquid chromatographs, an electrospray ionization source, and 6545 Q-TOF mass spectrometers. CPT was prepared at a concentration of 1 mg/mL in methanol, followed by centrifugation at 13000 g for 10 minutes to obtain the supernatant. Chromatographic separation was achieved on a Phenomenex Luna Omega column (100 A, 1.6 μm, 100 mm × 2.1 mm), maintaining the column temperature at 30℃, with an injection volume of 8 μL and a detection wavelength of 210 nm. The mobile phase consisted of 0.1% formic acid in water (A) and acetonitrile (B), following a gradient: 0-10 min, 60%-100% B; 10-15 min, 100% B; 15-16 min, 100%-60% B; 16-20 min, 60% B. The flow rate was set at 0.2 mL/min. ESI was performed in positive ion mode with a primary and secondary mass range of 100-1500 Da and 50-1500 Da, respectively. Additional parameters included a gas temperature of 350℃, gas flow of 11 L/min, sheath gas temperature of 350℃, sheath gas flow of 10 L/min, nebulizer pressure of 35 psi, the capillary voltage of 3500 V, nozzle voltage of 500 V, and collision voltages of 20, 40, 60, and 80 V. The identification of composition in CPT was based on molecular weight and characteristic fragmentation patterns.

2.3 Animals experiments

The HN rat experiments were previously detailed and depicted in Fig. 2A[28]. Male Sprague-Dawley rats (weight 200-220 g) were obtained from Hunan Slack Jingda Laboratory Animal Co., Ltd (Changsha, China, license number: SCXK (Xiang) 2019-0004). All animal experiments adhered to the Regulations of Experimental Animal Administration as approved by the Ethics Committee of the Institute of Chinese Medicine, Hunan Academy of Chinese Medicine. The rats were allocated into 4 groups (n = 6 per group): control group (Con), model group (Mod), benzbromarone group (Ben, 8.8 mg/kg), and CPT group (CPT, 150 mg/kg). The chosen dosage for CPT was based on the preliminary experimental results and literature reports[33, 34]. The HN rat model was induced through oral administration of adenine (150 mg/kg) and ethambutol (250 mg/kg) over 3 weeks. The interval between the modeling and oral administration is 5 h.

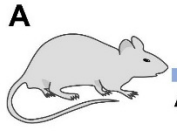

Group	9:00 am	2:00 pm
Con	0.5% CMC-Na	0.5% CMC-Na
Mod	250 mg/kg ethambutol 150 mg/kg adenine	0.5% CMC-Na
Ben	250 mg/kg ethambutol 150 mg/kg adenine	8.8 mg/kg benzbromarone
CPT	250 mg/kg ethambutol 150 mg/kg adenine	150 mg/kg CPT

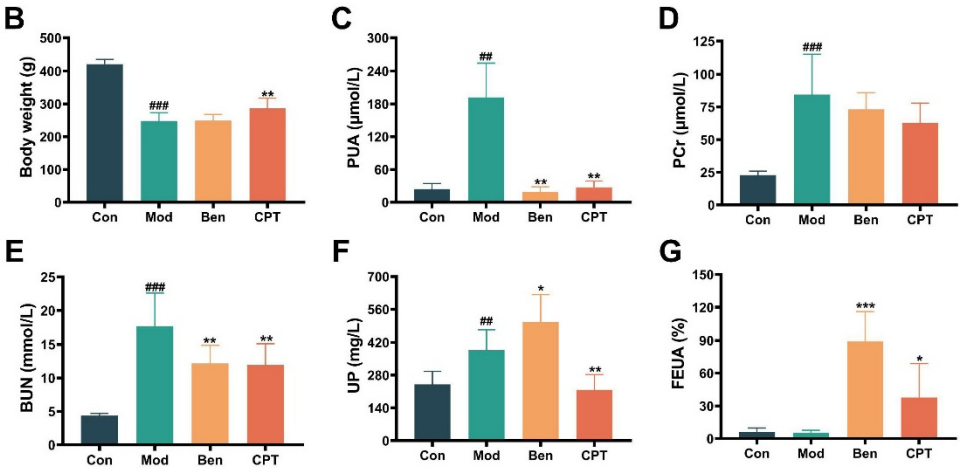

Fig. 2 CPT reduced PUA and improved renal function in HN rats. (A) The HN rats experimental procedure. (B) Body weight. (C) Plasma uric acid. (D) Plasma creatinine. (E) Plasma urea nitrogen. (F) Urine protein. (G) Fractional excretion of uric acid. Data are expressed as mean ± SD (n = 6). $^{\#\#}P < 0.01$, $^{\#\#\#}P < 0.001$ vs. the Con group; $^{*}P < 0.05$, $^{**}P < 0.01$, $^{***}P < 0.001$ vs. the Mod group. CPT: triterpenoids of *cyclocarya paliurus* leaves; PUA: plasma uric acid.

2.4 Plasma and urine biochemical analyses

The plasma levels of uric acid (PUA), creatinine (PCr), and urea nitrogen (BUN), along with the urine levels of uric acid (UUA), creatinine (UCr), and protein (UP), were measured by the respective kits. Subsequently, the fractional excretion of uric acid (FEUA) was calculated using the formula: FEUA (%) = [(UUA × PCr) / (PUA × UCr)] × 100%[28].

2.5 Histopathological and immunohistochemistry analyses

The procedure for hematoxylin-eosin (HE), Masson's trichrome (MTS), and immunohistochemical (IHC) staining of renal tissues has been delineated in previous work[28]. The picro sirius red (PSR) staining of renal sections was performed to detect the collagen fibers. The stained sections were observed using optical microscopy at 200 × magnification. For semi-quantitative assessments, five fields were randomly selected. The extent of renal fibrosis in MTS-stained sections was quantified using the formula: kidney fibrosis area (%) = positive area/tissue area. Additionally, the Average Integrated Optical Density (AIOD) for IHC-stained sections was determined by the following calculation: AIOD = integrated optical density/tissue area. Measurements of the positive area, tissue areas, and integrated optical densities were conducted using ImageJ software.

2.6 Plasma metabolomics and kidney proteomics

The methodology for the plasma non-targeted metabolomics and label-free kidney proteomics adhered to the protocols delineated in a previous study[28]. Differentially expressed proteins (DEPs) were filtered using the following criteria: fold change (FC) > 1.2 or < 0.83, and *P*-value < 0.05.

2.7 Network pharmacological analysis and molecular docking

The network pharmacological analysis was performed according to the reported literatures[37, 38]. The human targets of CPT were predicted by the SwissTargetPrediction database (http://swisstargetprediction.ch/). The HN targets were aggregated from GeneCards

(https://www.genecards.org/), HERB (http://herb.ac.cn), DisGeNET (https://www.disgenet.org/), and OMIM (https://www.omim.org/) databases using “hyperuricemia nephropathy”, “urate nephropathy”, and “uric acid nephropathy” terms. The intersecting targets were obtained through a Venn diagram, which were considered as targets for CPT treatment of HN. These intersecting targets were subsequently input into the String (https://cn.string-db.org/) database to construct a protein-protein interaction (PPI) network, where the top 20 targets with high degree value were considered as core targets. Further analysis employed Cytoscape 3.9.1 to develop a compound-target network. Functional enrichment analysis was conducted using the David (https://david.ncifcrf.gov/) database for GO and KEGG analysis. Molecular docking procedures were carried out with Autodock Vina. The structure of targets (STAT3: 6NJS; IL-2: 1M49; CASP1: 1RWM; EGFR: 1XKK; REN: 2BKS) was obtained from the PDB (https://www.rcsb.org/) database. Compound energy minimization was computed via the MMFF94 force field, with PyMol used for result visualization.

2.8 Cell culture and treatment

HK-2 cells were cultured under standard conditions in DMEM/F12 medium supplemented with 10% fetal bovine serum, maintained at 37℃ and 5% CO_2. UA-induced HK-2 cell experiments were performed following previous reports with some modifications[22, 39]. HK-2 cells were plated in 96-well plates at a density of 1×10^4 per well and subjected to varied concentrations of UA or CPT for 24 or 48 h. The viability of cells was assessed using the Cell Counting Kit-8 (CCK-8), where, after a 2 h incubation period with the CCK-8 solution, the absorbance was measured at 450 nm. For western blot analysis, HK-2 cells were seeded into 6-well plates at a density of 2×10^5 cells/well. Following 12 h of serum starvation, cells were treated with 0.6 mg/mL UA with or without CPT for 48 h. Protein lysates were then harvested for western blot analysis.

2.9 Cellular thermal shift assay and surface plasmon resonance

Cellular thermal shift assay (CETSA) and surface plasmon resonance (SPR) were used to detect the interaction between samples and STAT3. HK-2 cells were harvested, and the protein supernatant was separated by centrifugation (10000 g, 10 min, 4℃) after three freeze-thaw cycles. The supernatant was divided into control and experimental groups treated with DMSO, CPT (50 μg/mL), or cypaliuruside B (CYB, 20 μmol/L, isolated from CPT; the ^1H and ^{13}C NMR data were shown in Figs. S1 and S2) for 2h at 4℃, respectively. The samples were subjected to thermal stress at temperatures ranging between 40℃ and 65℃ for 4 min. After centrifugation, supernatants were collected for analysis via electrophoresis and Western blotting. SPR was performed in a Biacore 8K instrument (GE Healthcare, USA). STAT3 protein (50 μg/mL) was immobilized onto a CM5 Sensor Chip (Cytiva, USA) using amine coupling procedures, achieving approximately 11845 RU. Phosphate-buffered saline (PBS) containing 1% DMSO served as the running buffer during immobilization. Following immobilization, the CYB solution was prepared by diluting the stock solution with PBS containing 5% DMSO. Five concentrations of the CYB solution were injected sequentially at a flow rate of 30 μL/min, with the binding phase lasting for 150 s at 25℃.

Experimental data were collected and analyzed using Biacore Insight software (Cytiva, USA) to fit an appropriate binding model and determine the equilibrium dissociation constant.

2.10 ELISA and western blot analyses

Kidney tissues (50 mg) were homogenized in 500 μL of phosphate-buffered saline at 4℃. The supernatant was collected following centrifugation at 10000 g for 10 minutes at 4℃. Levels of rat TNF-α, IL-6, and TGF-β1 in the supernatant were quantified using ELISA kits. For Western blot analysis, the procedure mirrored that previously described[28]. Membranes were incubated with primary antibodies overnight at 4℃, diluted as follows: GAPDH, 1:50000; URAT1, 1:2000; OAT1, 1:1000; GLUT9, 1:5000; IL-6, 1:2000; COLIA1, 1:1000; α-SMA, 1:20000; vimentin, 1:20000; e-cadherin, 1:5000; STAT3, 1:2000; p-STAT3, 1:10000; SOCS3, 1:5000; PARL, 1:1000; CSRP2, 1:2000.

2.11 Dual-Luciferase Reporter Assay

The STAT3 binding sites in the CSRP2 and PARL promoter regions (the 2000 bp promoter sequences upstream of the translation initiation sites) were predicted with the JASPAR database (https://jaspar.elixir.no/). The dual-luciferase reporter assay was employed to validate the binding between STAT3 and the CSRP2 promoter. pRL-TK, STAT3-OE, and pGL3-Basic (containing the CSRP2 promoter sequence) were cotransfected into HEK-293T cells with DNA transfection reagent (Neofect biotech Co.,Ltd. Beijing, China). The luciferase activity was detected 24 hours post-transfection with the corresponding kit (Yeasen Biotechnology Co., Ltd., Shanghai, China).

2.12 Statistical analysis

Data are presented as the mean ± standard deviation. Statistical analyses were conducted using SPSS software (version 27.0). Group differences were assessed for statistical significance using one-way ANOVA followed by the LSD test (when the variances were uniform) or the Dunnett T3 test (when the variances were not uniform). The value of $P < 0.05$ was considered statistically significant.

3. Results

3.1 Phytochemical analysis of CPT

The mass fragment ion of pterocaryoside A, pterocaryoside B, cyclocarioside P, cyclocarioside D, cyclocarioside F, cyclocarioside I, and cyclocarioside Z9, isolated from *C. paliurus* leaves by our research group, revealed that 3,4-seco-dammarane triterpenoids generated specific fragment ions (Fig. S3). For example (Figs. 1A and B), the $[M+Na]^+$ at *m/z* 673.43 for cyclocarioside D produced $[M+Na\text{-}Qui]^+$ and $[Qui+Na]^+$ ions at *m/z* 509.36 and 187.06 through glycosidic bond cleavage, respectively. Further fragmentation of the *m/z* 509.36 ion yielded ions at *m/z* 477.33 and 395.25, following the neutral loss of CH_3OH and $C_7H_{14}O$. Additionally, the total ion chromatogram for CPT is illustrated in Fig. 1C. By correlating these fragmentation patterns with those of standard or previously reported compounds, a total number of 34 triterpenoids were identified from CPT, including nineteen 3,4-seco-dammarane triterpenoids,

twelve dammarane triterpenoids, two oleanane triterpenoids, and one nor-dammarane triterpenoid (Fig. 1D and Table S1). Notably, the total triterpenoid content of CPT was quantified at 78.33%[28].

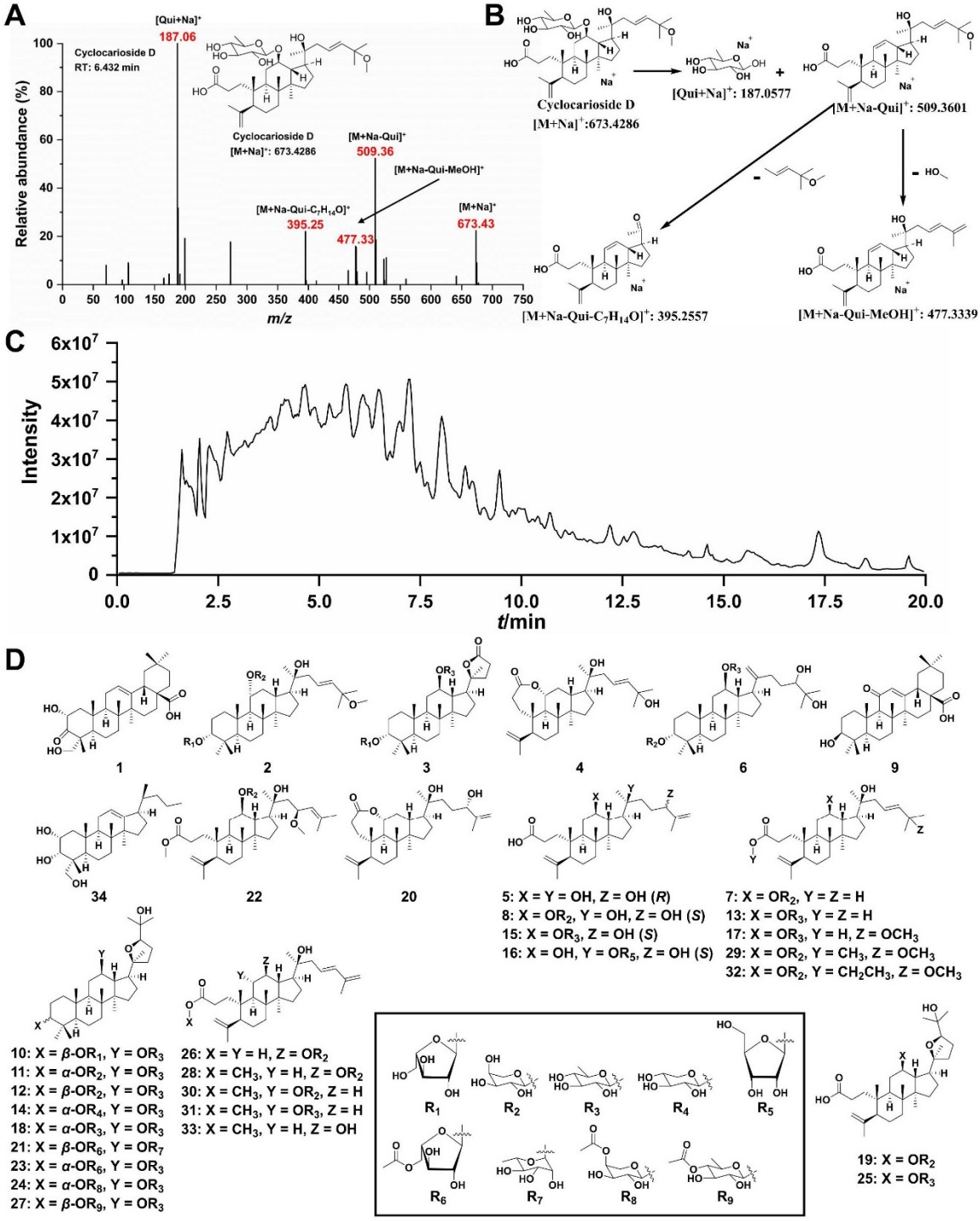

Fig. 1 Chemical composition analysis of CPT by HPLC-ESI-Q-TOF-MS/MS. (A) The MS/MS spectrum of cyclocarioside D. (B) The speculative fragmentation pathway of cyclocarioside D. (C) Total ion chromatograms of CPT in positive ion mode. (D) Structures of the triterpenoids identified from CPT. CPT: triterpenoids of *cyclocarya paliurus* leaves.

3.2 CPT reduced PUA levels and improved renal function in HN rats

Administration of 150 mg/kg adenine and 250 mg/kg ethambutol for three weeks led to a reduction in body weight and elevated levels of PUA, PCr, BUN, and UP in the Mod group compared to the Con group (Figs. 2B-G). These results confirm the successful establishment of the HN rat model. As anticipated, CPT mitigated weight loss associated with HN and decreased levels of PUA, BUN, and UP, slightly reduced PCr

levels, and enhanced FEUA. Conversely, benzbromarone markedly reduced PUA and BUN levels, augmented UP content, and increased FEUA, without affecting body weight.

3.3 CPT ameliorated renal inflammation and fibrosis in HN rats

Hyperuricemia can lead to urate deposition in the kidneys, subsequently causing renal inflammation and tubulointerstitial fibrosis[19]. As depicted in Figs. 3A and B, in the Mod group, TNF-α and IL-6 levels in the kidneys were higher compared to the Con group. Remarkably, both CPT and benzbromarone effectively decreased TNF-α and IL-6 levels in HN rats. Additionally, CPT significantly lowered TGF-β1 level (Fig. 3C). HE staining revealed that the kidneys in the Mod group exhibited severe pathological changes, including renal tubular atrophy, narrowing of tubular lumens, epithelial degeneration, tubular dilation, urate crystal deposition with surrounding multinucleated giant cells, and lymphocyte infiltration (Fig. 3D). Notably, CPT ameliorated these lesions to varying degrees. Conversely, benzbromarone only mitigated urate crystal deposition. MTS and PSR staining (Figs. 3D and E) and western blot analyses (Figs. 3F-H) indicated a significant increase in collagen deposition and the expression of fibrosis markers, such as α-SMA and COL1A1, in the kidneys of HN rats. CPT significantly reduced renal collagen deposition and decreased the levels of α-SMA and COL1A1 in HN rats, whereas benzbromarone had no effect on these fibrosis markers.

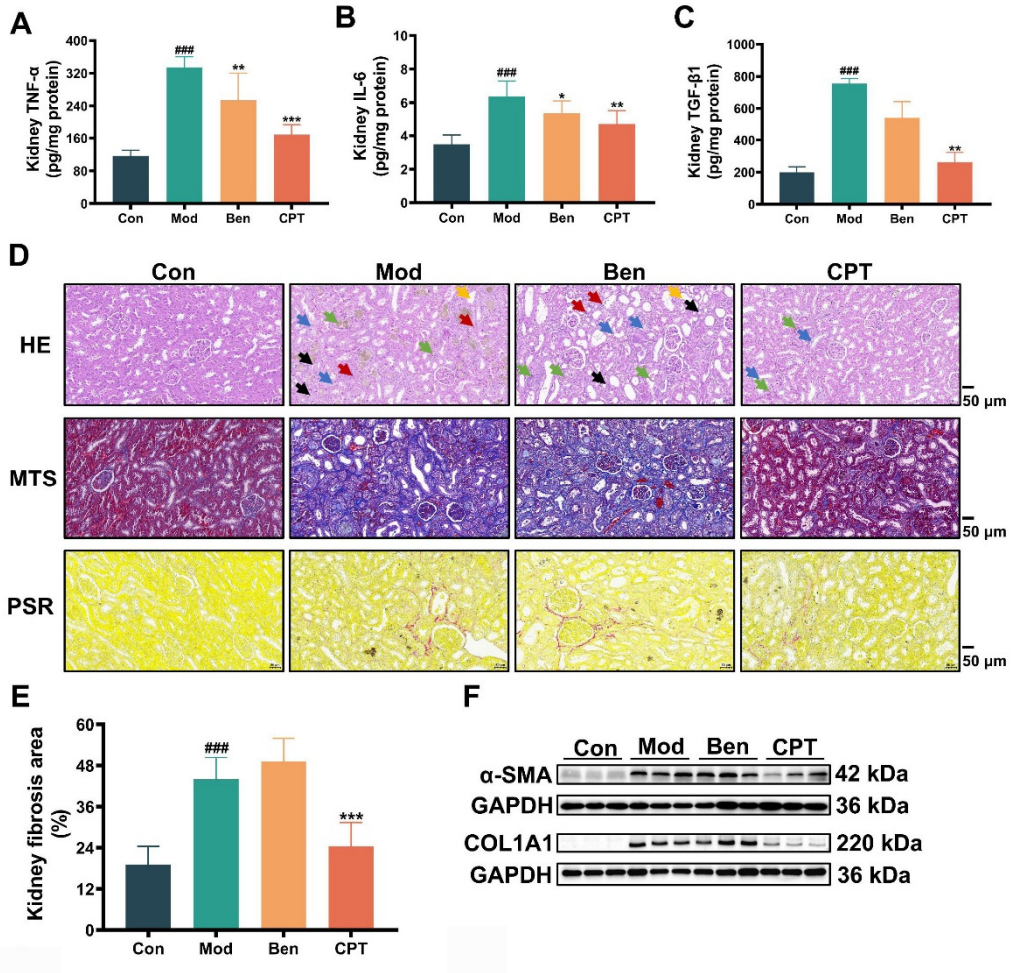

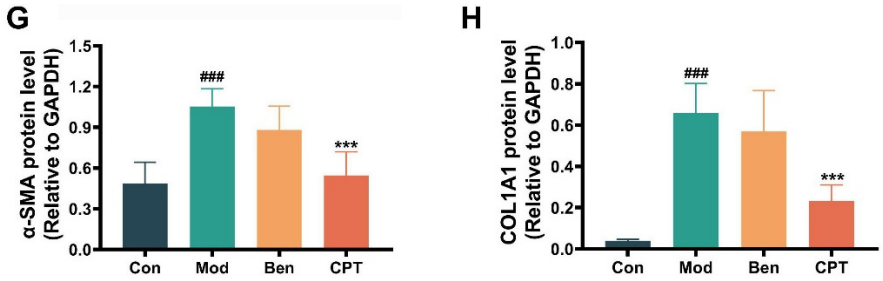

Fig. 3 CPT ameliorated renal inflammation and fibrosis in HN rats. (A-C) Kidney TNF-α, IL-6, and TGF-β. (D) The HE, MTS, and PSR staining of kidney tissues (magnification × 200, scale bar 50 μm). The red arrow represents dotted infiltration of interstitial lymphocytes; the black arrow represents renal tubules atrophy and luminal stenosis; the blue arrow represents renal tubular epithelial cell degeneration; the yellow arrow represents the dilated renal tubules; the green arrow represents urate crystal deposition with multinucleated giant cells around. (E) Kidney fibrosis area. (F) Western blot analysis of α-SMA and COL1A1. (G and H) Quantification of α-SMA and COL1A1. Data are expressed as mean ± SD (n = 6). $^{###}P < 0.001$ vs. the Con group; $^{*}P < 0.05$, $^{**}P < 0.01$, $^{***}P < 0.001$ vs. the Mod group. CPT: triterpenoids of *cyclocarya paliurus* leaves; HE: hematoxylin-eosin staining; MTS: masson's trichrome staining; PSR: picro sirius red staining.

3.4 CPT restored purine metabolism in HN rats

The PCA score plots in both positive and negative modes distinctly separated the plasma metabolic profiles of the Mod, Con, and CPT groups, demonstrating that CPT rectified the metabolic imbalances caused by HN (Figs. 4A and B). Subsequently, based on the differential metabolite criteria: VIP (variable importance in the projection of OPLS-DA) > 1 and $P < 0.05$, CPT reversed 36 metabolites (Fig. 4C, and Table S2). These metabolites were associated with various metabolic processes, including arginine biosynthesis, purine metabolism, and riboflavin metabolism, as indicated by KEGG analysis (Fig. 4D). Disordered purine metabolism is a pivotal characteristic and underlying cause of HN (Fig. 4E). After being given adenine and ethambutol, the levels of adenine, inosine, hypoxanthine, guanine, deoxyguanosine, UA, and allantoin related to purine metabolism in the plasma of HN rats were significantly increased. Simultaneously, CPT decreased the levels of adenine, inosine, hypoxanthine, uric acid, and allantoin, indicating that CPT inhibited overactivated purine metabolism in HN rats.

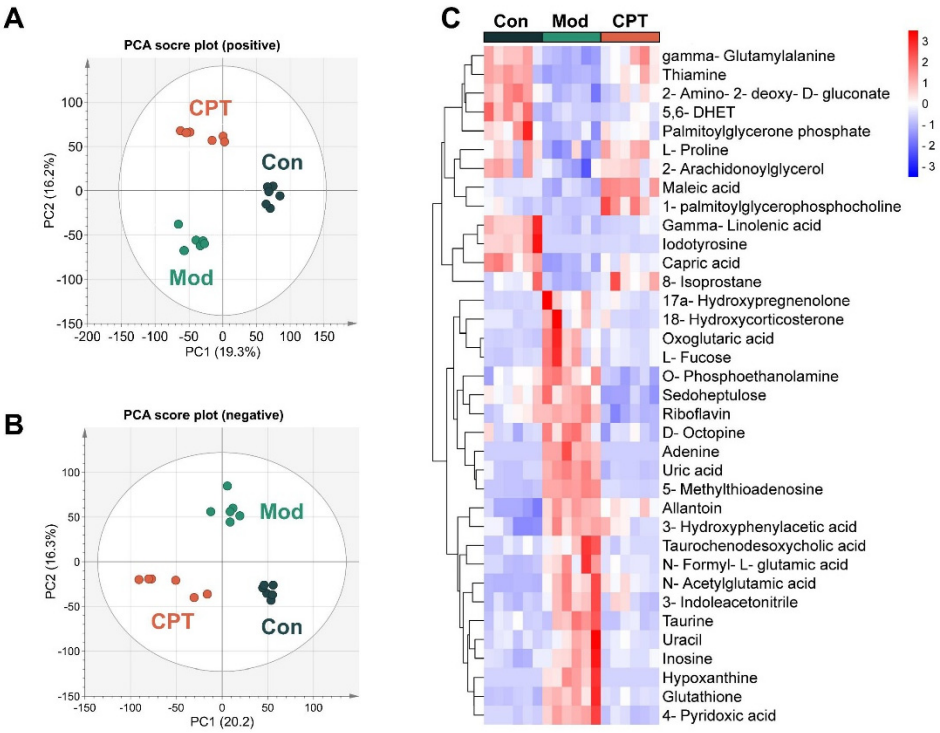

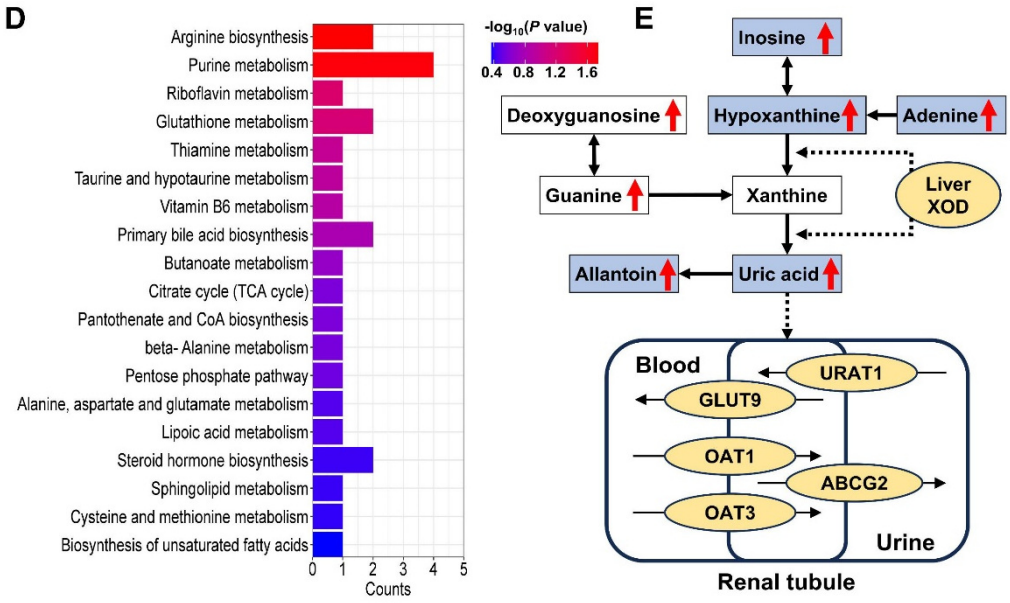

Fig. 4 The plasma non-targeted metabolomics analysis. (A and B) PCA score plots of positive and negative modes. (C) Heatmap of reversed metabolites. (D) KEGG analysis of reversed metabolites. (E) Purine metabolism. The red arrow indicates the metabolite level was increased in the Mod group. The blue box represents the metabolite level was reversed by CPT. CPT: triterpenoids of *cyclocarya paliurus* leaves.

3.5 CPT regulated renal urate transporters in HN rats

The generation and excretion of UA maintain the level of UA in the body (Fig. 4E). The hepatic XOD activity and expression in the Mod group were significantly increased compared to the Con group, while CPT and benzbromarone did not affect hepatic XOD activity and expression (Figs. 5A and B). On the other hand, CPT may promote urate excretion through the kidney (Fig. 2G). Western blot analysis showed that the renal URAT1 and GLUT9 levels were upregulated, while the OAT1 level was downregulated in the HN rats. Treatment with CPT and benzbromarone resulted in the downregulation of renal URAT1 and GLUT9 levels, with CPT uniquely inducing the upregulation of OAT1 levels (Figs. 5C-F). Immunohistochemical results corroborated those of the western blot analysis (Figs. 5G-J).

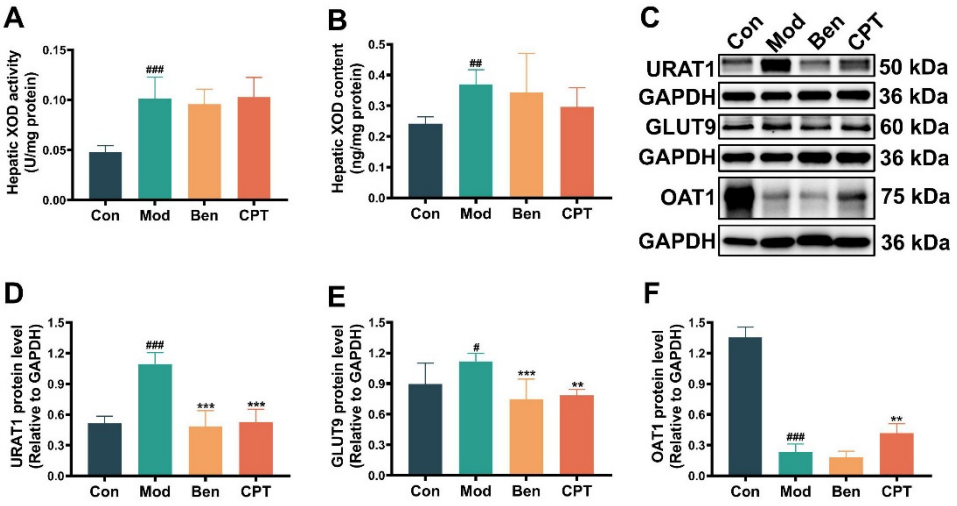

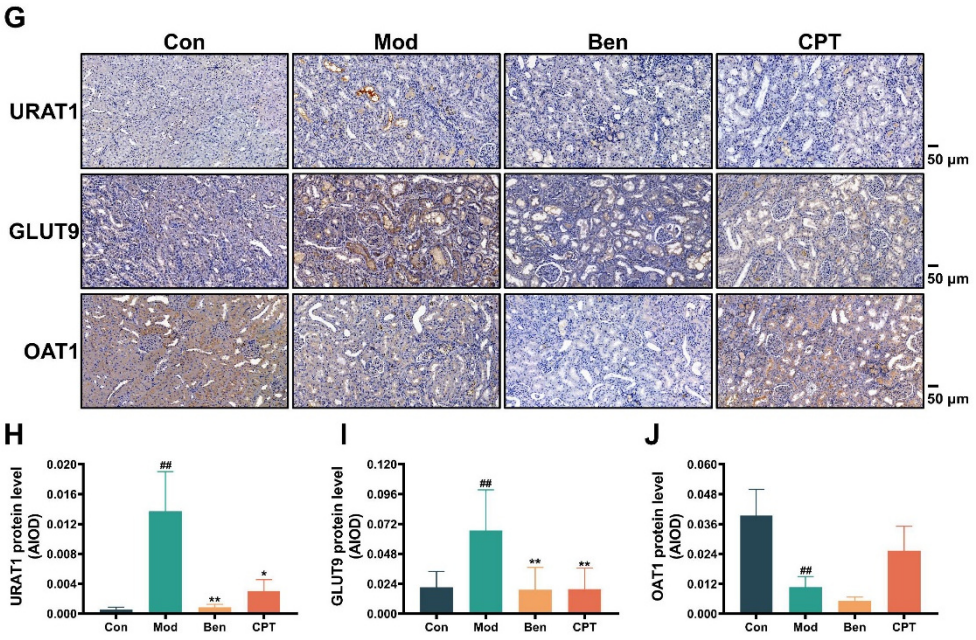

Fig. 5 CPT regulated renal urate transporters in HN rats. (A and B) Hepatic XOD activity and content. (C) Western blot analysis of renal URAT1, GLUT9, and OAT1. (D-F) Quantitative analysis results of western blot analysis in (C). (G) Immunohistochemistry analysis of renal URAT1, GLUT9, and OAT1. (H-J) AIOD quantification of renal URAT1, GLUT9, and OAT1. Data are expressed as mean ± SD (n = 6). $^{\#}P < 0.05$, $^{\#\#}P < 0.01$, $^{\#\#\#}P < 0.001$ vs. the Con group; $^{*}P < 0.05$, $^{**}P < 0.01$, $^{***}P < 0.001$ vs. the Mod group. CPT: triterpenoids of *cyclocarya paliurus* leaves; HN: hyperuricemic nephropathy.

3.6 CPT downregulated renal PARL and CSRP2 in HN rats

Label-free proteomics was utilized to unveil additional mechanisms of CPT in mitigating HN. Compared with the Con group, a total of 418 proteins were upregulated and 783 proteins were downregulated in the Mod group (Fig. 6A). Compared with the Mod group, CPT downregulated 185 proteins and upregulated 138 proteins (Fig. 6B). After taking the intersection, CPT reversed the expression of 35 proteins in HN rats (Fig. 6C and Table S3). These reversed proteins were associated with the regulation of cell adhesion, ER calcium ion concentration reduction, mitochondrial calcium ion concentration elevation, and cytoskeleton organization (Fig. S4). PARL and CSRP2 are closely related to renal injury and fibrosis. Proteomics and western blot analyses showed that CPT downregulated the elevated levels of PARL and CSRP2 caused by HN (Figs. 6D-H).

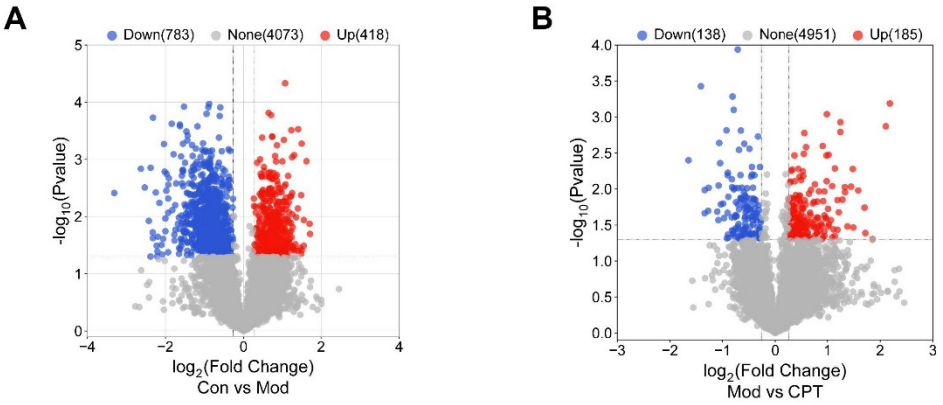

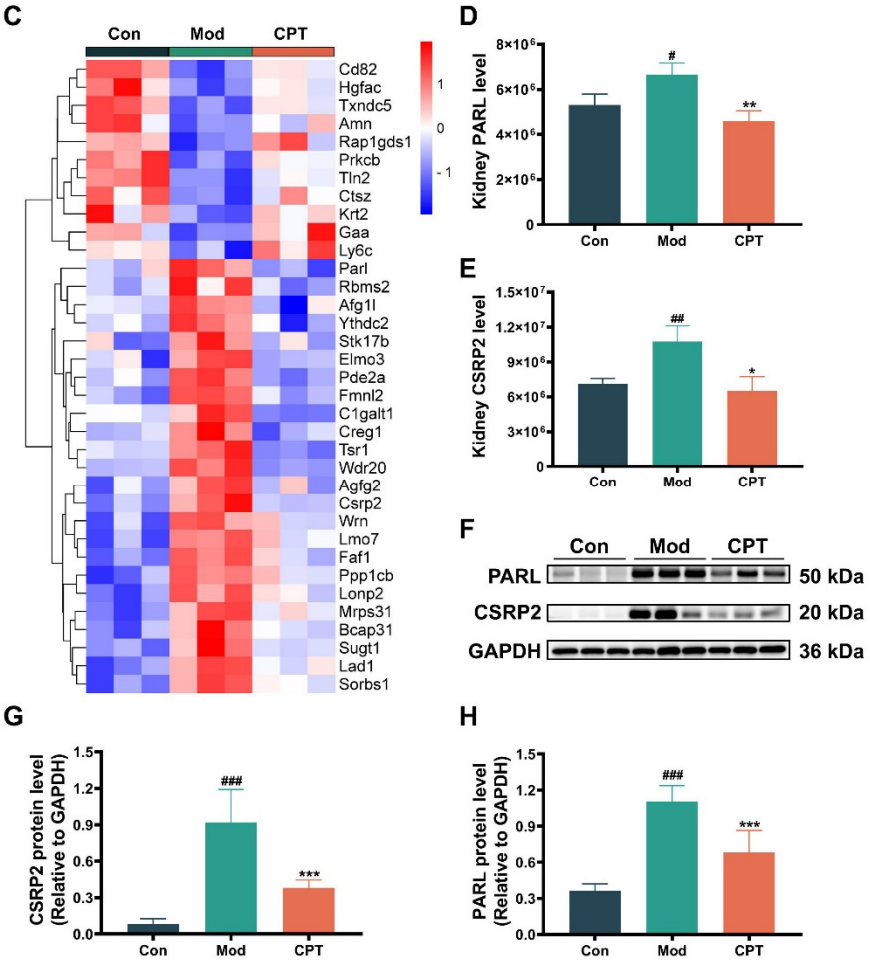

Fig. 6 The kidney label-free proteomics analysis. (A) Volcano plot of Con *vs* Mod. (B) Volcano plot of Mod vs CPT. (C) Heatmap of reversed proteins. (D and E) Quantification of PARL and CSRP2 from proteomics (n = 3). (F) Western blot analysis of renal PARL and CSRP2. (G and H) Quantification of western blot analysis in (F, n = 6). Data are expressed as mean ± SD. $^{\#}P < 0.05$, $^{\#\#}P < 0.01$, $^{\#\#\#}P < 0.001$ vs. the Con group; $^{*}P < 0.05$, $^{**}P < 0.01$, $^{***}P < 0.001$ vs. the Mod group. CPT: triterpenoids of *cyclocarya paliurus* leaves.

3.7 Network pharmacology and molecular docking analysis

Network pharmacology analysis was conducted to investigate the mechanism of CPT in improving nephropathy induced by hyperuricemia. A total of 496 targets for CPT were acquired, and 1681 therapeutic targets of HN were collected from public databases after deduplication (Fig. 7A). An intersection of 168 targets was found between the predicted CPT targets and the therapeutic HN targets (Fig. 7A). GO and KEGG enrichment analyses have revealed that these intersecting targets are implicated in numerous pathways, such as PI3K-Akt, MAPK, and TNF-α pathways (Fig. S5). The PPI network analysis, considering the degree value and the triterpenoids' associations through topological assessments, highlighted STAT3, renin (REN), IL-2, caspase-1 (CASP1), and epidermal growth factor receptor (EGFR) as primary targets (Figs. 7B and C). Specifically, 22 triterpenoids in CPT, comprising fifteen 3,4-seco-dammarane and seven dammarane triterpenoids, were targeting STAT3 (Fig. 7D). Molecular docking revealed that these triterpenoids exhibited strong binding to STAT3 (binding energy < -5 kcal/mol). For example, compound 6 (dammarane) established six hydrogen bonds with four STAT3 residues (Fig. 7E, SER-636, ARG-609, SER-611, and SER-613, binding energy = -8.414 kcal/mol). In comparison, compound 19

(3,4-seco-dammarane) formed four hydrogen bonds with three residues (Fig. 7F, ARG-609, GLU-594, and GLU-612, binding energy = -6.630 kcal/mol). Moreover, additional triterpenoids demonstrated favorable interactions with REN, IL-2, CASP1, and EGFR (Fig. S6), proposing that IL-6/STAT3 and its related pathways could be crucial for CPT against HN.

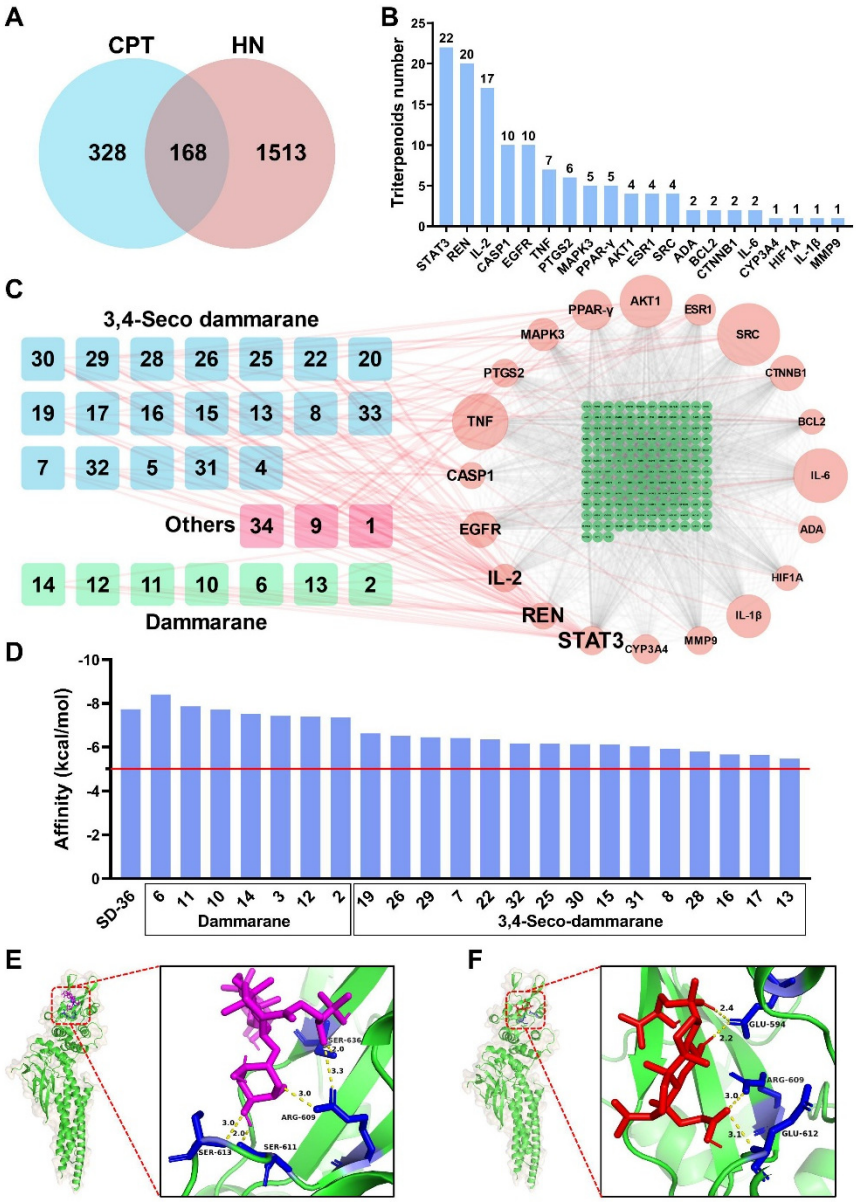

Fig. 7 Network pharmacological and molecular docking analyses. (A) The Venn diagram between predicted targets for CPT with HN therapeutic targets. (B) The core targets of CPT in treating HN. (C) The triterpenoids-targets interaction network. (D) The binding energy between triterpenoids with STAT3 (PDB: 6NJS). (E) The visualization of compound 6 with STAT3. (F) The visualization of compound 19 with STAT3. CPT: triterpenoids of *cyclocarya paliurus* leaves; HN: hyperuricemic nephropathy.

3.8 CPT inhibited renal EMT and IL-6/STAT3/SOCS3 signaling pathway in HN rats

Given the observed lack of substantial improvement in renal injury with benzbromarone treatment, subsequent investigations focused exclusively on the mechanisms by which CPT ameliorates HN. α-SMA is upregulated during EMT and can serve as a biomarker for renal fibrosis[17]. Moreover, IL-6 exacerbates renal inflammation and tissue damage by activating the STAT3 signaling pathway[15, 17]. As shown in Figs.

8A-C, the renal expression of E-cadherin was downregulated, whereas vimentin was upregulated in the Mod group compared to the Con group. Notably, the administration of CPT reversed the expression of E-cadherin and vimentin. Additionally, increases in IL-6, p-STAT3, SOCS3, and the p-STAT3/STAT3 ratio were noted in the HN rats. Crucially, the CPT treatment reduced the renal levels of IL-6, p-STAT3, STAT3, SOCS3, and the p-STAT3/STAT3 ratio in comparison to the Mod group (Figs. 8D-H).

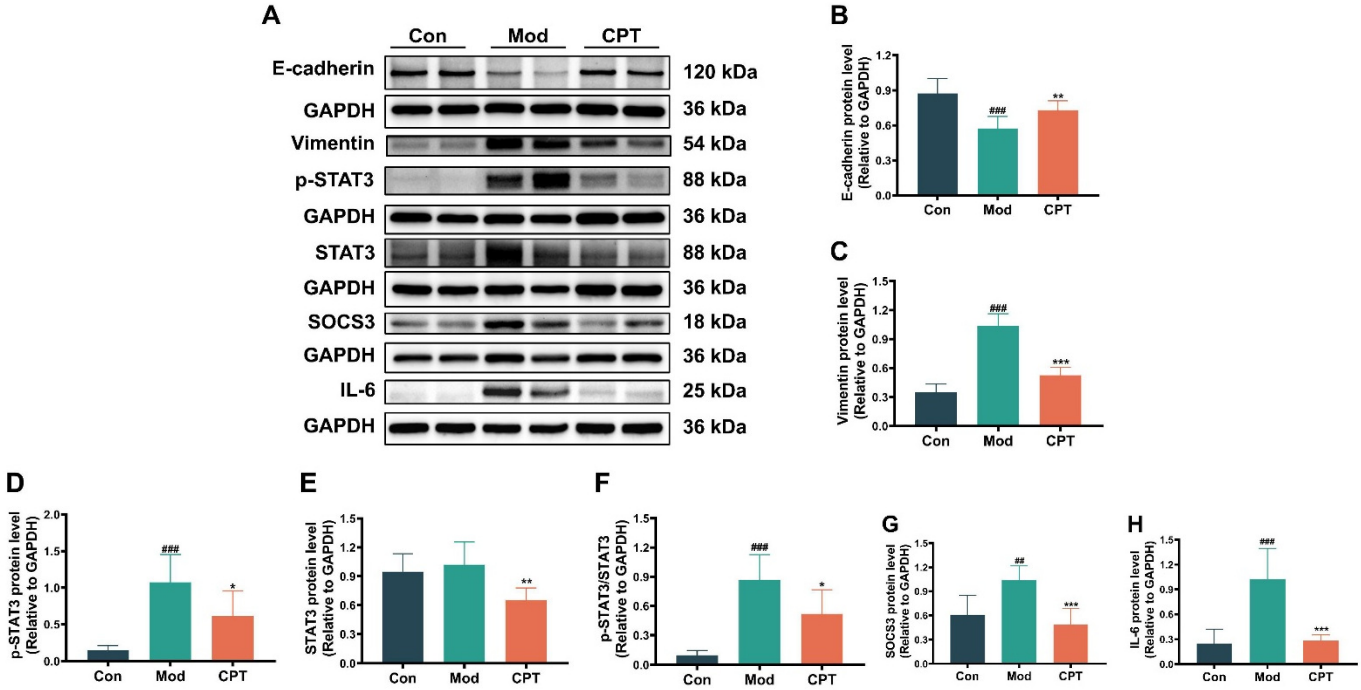

Fig. 8 CPT inhibited renal EMT and IL-6/STAT3/SOCS3 signaling pathway in HN rats. (A) Western blot analysis of renal E-cadherin, vimentin, p-STAT3, STAT3, SOCS3, and IL-6. (B-H) Quantitative analysis results of western blot analysis in (A). Data are expressed as mean ± SD (n = 6). $^{\#\#}P < 0.01$, $^{\#\#\#}P < 0.001$ vs. the Con group; $^{*}P < 0.05$, $^{**}P < 0.01$, $^{***}P < 0.001$ vs. the Mod group. CPT: triterpenoids of *cyclocarya paliurus* leaves; HN: hyperuricemic nephropathy.

3.9 CPT inhibited the dysfunction of HK-2 cells induced by UA through binding with STAT3

UA-induced HK-2 cells model is a commonly used *in vitro* HN model[22, 39]. CCK-8 assay results revealed that UA significantly reduced HK-2 cell viability to less than 90% at a concentration of 0.6 mg/mL over 48 h, thus, HK-2 cells were induced by 0.6 mg/mL UA for 48 h to construct an *in vitro* HN model (Fig. 9A). Moreover, CPT exhibited no adverse effects on HK-2 cell activity at concentrations up to 25 μg/mL (Fig. 9B). After UA stimulation, the expression of IL-6, p-STAT3, SOCS3, α-SMA, and the ratio of p-STAT3 to STAT3 in HK-2 cells increased, while the expression of E-cadherin significantly decreased, indicating that UA activated the IL-6/STAT3/SOCS3 signaling pathway and promoted EMT. Similar to *in vivo* results, CPT reversed the expression of IL-6, SOCS3, α-SMA, and vimentin, and reduced the ratio of p-STAT3 to STAT3 in UA-induced HK-2 cells (Figs. 9C-E). CPT eliminated the elevated levels of PARL and CSRP2 in UA-induced HK-2 cells (Figs. 9C-E). CETSA showed that CPT increased the thermal stability of STAT3, further confirming that components within CPT could bind to STAT3 (Fig. 10A). Additionally, CETSA demonstrated that cypaliuruside B (a seco-triterpenoid isolated from CPT, Fig. 10B) binds to STAT3 (Fig. 10C). Furthermore, SPR analysis revealed that CYB binds to STAT3 with moderate affinity, exhibiting a dissociation constant (K_D) of 7.32 μmol/L (Fig. 10D). At concentrations that did not

affect cell viability (Fig. S7), S3I-201 (25 μmol/L, a STAT3 inhibitor) significantly inhibited the UA-induced expression of p-STAT3, STAT3, α-SMA, and CSRP2 in HK-2 cells, but had no effect on PARL. In contrast, both CPT (25 μg/mL) and CYB (20 μmol/L) significantly inhibited the expression of p-STAT3, α-SMA, CSRP2, and PARL in the UA-induced HK-2 cell model (Figs. 10E-J). The inhibitory effects of CPT and CYB on α-SMA and CSRP2 were attenuated after administration of Colivelin (5 μmol/L, a STAT3 agonist) (Figs. 11A-F). Therefore, CPT and CYB ameliorated UA-induced HK-2 cell injury by inhibiting STAT3. Concurrently, a potential association was observed between STAT3 and CSRP2. JASPAR prediction analysis indicated that STAT3 binds to the CSRP2 promoter, while its binding affinity for the PARL promoter was relatively weak (Fig. 11G). Then, dual-luciferase reporter assays confirmed the ability of STAT3 to bind to the CSRP2 promoter, as in co-transfection assays, the overexpression of STAT3 strengthened the activity of the CSRP2 promoter (Fig. 11H).

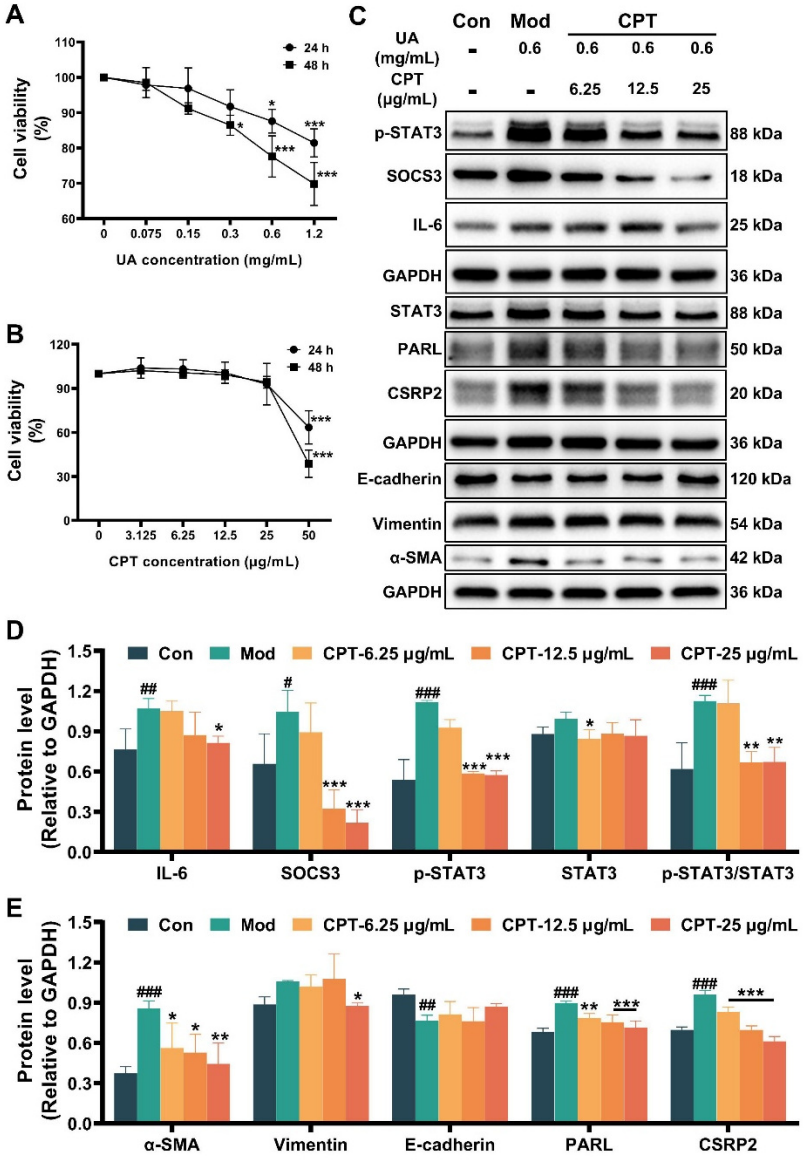

Fig. 9 CPT inhibited the dysfunction of HK-2 cells induced by UA. (A) Effect of UA on HK-2 cell viability. (B) Effect of CPT on HK-2 cell viability. (C) Western blot analysis of p-STAT3, SOCS3, IL-6, STAT3, PARL, CSRP2, E-cadherin, vimentin, and α-SMA in UA-induced HK-2 cells. (D) Quantification of IL-6, SOCS3, p-STAT3, STAT3, and the ratio of p-STAT3 to STAT3. (E) Quantification of α-SMA, vimentin, E-cadherin, PARL, and CSRP2. Data are expressed as mean ± SD (n = 3). $^{\#}P < 0.05$, $^{\#\#}P < 0.01$, $^{\#\#\#}P < 0.001$ vs. the Con group; $^{*}P < 0.05$, $^{**}P < 0.01$, $^{***}P < 0.001$ vs. the Mod group. CPT: triterpenoids of *cyclocarya paliurus* leaves; UA: uric acid.

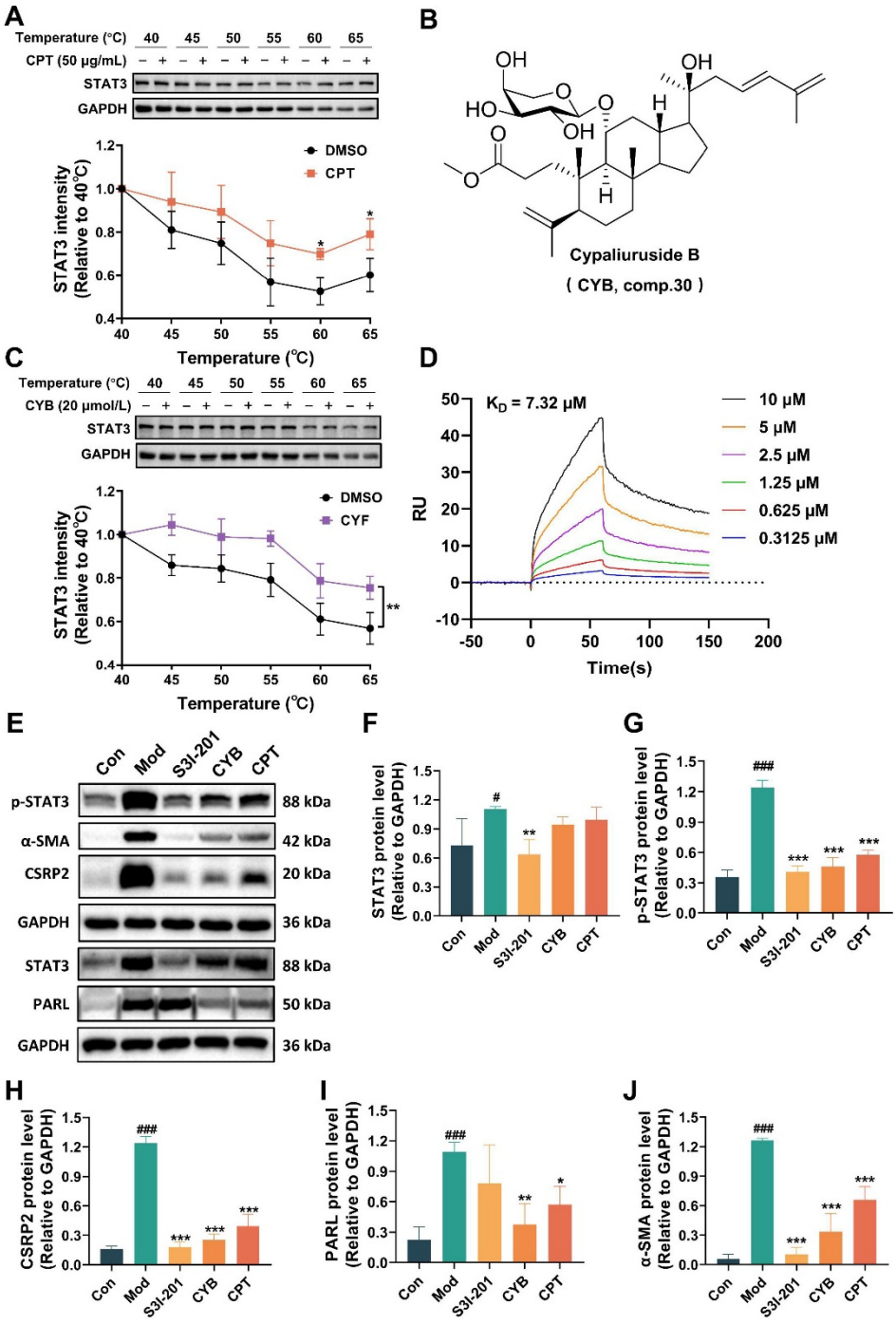

Fig. 10 CPT and CYB bind with STAT3. (A) CETSA analysis to verify CPT binding to STAT3 (n = 3). (B) The structure of CYB. (C) CETSA analysis to verify CYB binding to STAT3 (n = 3). (D) SPR analysis to verify CYB binding to STAT3. (E) Western blot analysis of p-STAT3, STAT3, α-SMA, PARL, and CSRP2 in UA-induced HK-2 cells affected by S3I-201 (25 μmol/L), CYB (20 μmol/L), and CPT (25 μg/mL) (F-J) Quantification of p-STAT3, STAT3, α-SMA, PARL, and CSRP2 (n = 4). Data are expressed as mean ± SD. $^{\#}P < 0.05$, $^{\#\#\#}P < 0.001$ vs. the Con group; $^{*}P < 0.05$, $^{**}P < 0.01$, $^{***}P < 0.001$ vs. the Mod group. CPT: triterpenoids of *cyclocarya paliurus* leaves; CYB: cypaliuruside B.

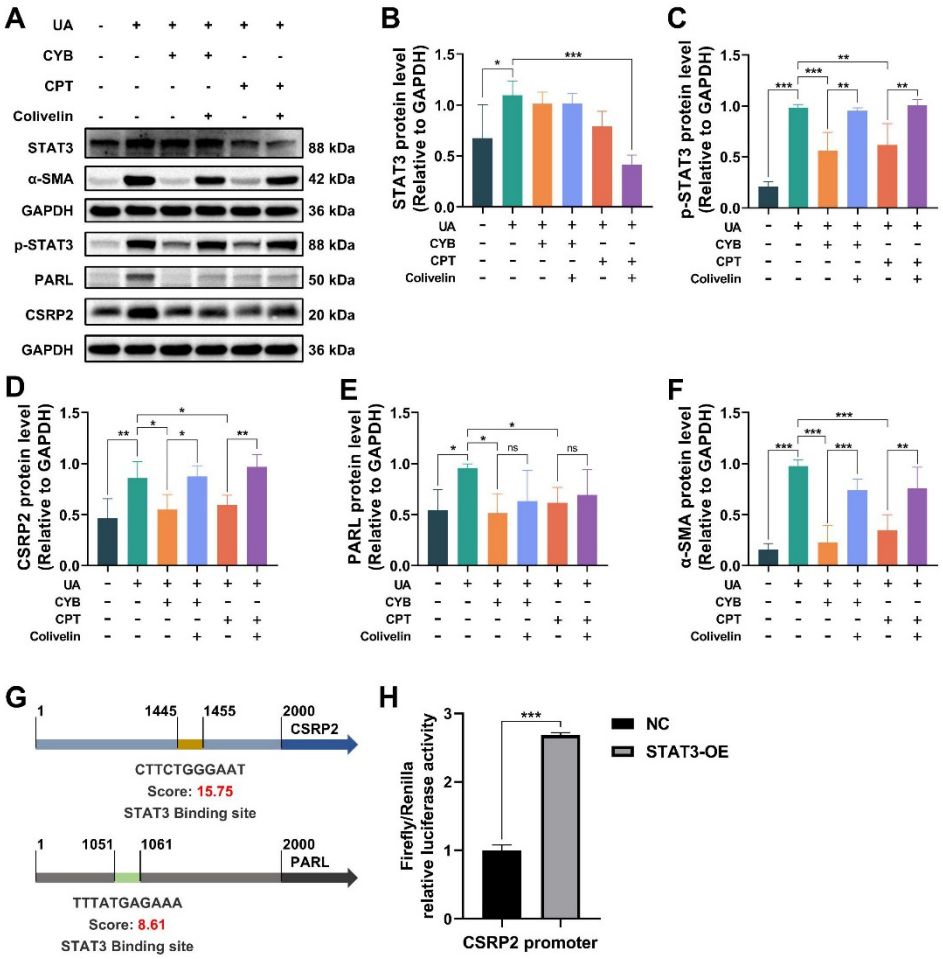

Fig. 11 STAT3 activation attenuated the effects of CPT and CYB in HK-2 cells induced by UA. (A) Western blot analysis of p-STAT3, STAT3, α-SMA, PARL, and CSRP2 in UA-induced HK-2 cells affected by colivelin (5 μmol/L) with CYB (20 μmol/L) or CPT (25 μg/mL). (B-F) Quantification of STAT3, p-STAT3, CSRP2, PARL, and α-SMA. Data are expressed as mean ± SD (n = 3). (G) Prediction of STAT3-binding sites in the CSRP2 and PARL promoter regions. (H) Dual-luciferase reporter assay analyzing the interaction between STAT3 with CSRP2 (n = 4). Data are expressed as mean ± SD. $^{*}P < 0.05$, $^{**}P < 0.01$, $^{***}P < 0.001$; ns: non-significant. CPT: triterpenoids of *cyclocarya paliurus* leaves; CYB: cypaliuruside B.

4. Discussion

HN has an increased risk of progression to end-stage renal disease, with therapeutic drugs currently insufficient. Triterpenoids, characteristic active compounds found in *C. paliurus*, exhibit notable efficacy in ameliorating glycolipid metabolic disorders such as diabetic nephropathy and NAFLD[32-36]. The effects and mechanisms of CPT on HN have yet to be reported. This study demonstrated that CPT significantly reduced PUA levels and alleviated renal inflammation and fibrosis in HN rats. Subsequently, plasma non-targeted metabolomics and renal urate transporters assays indicated that CPT improved purine metabolism by modulating the expression of renal urate transporters. Network pharmacology, molecular docking, renal proteomics, dual-luciferase reporter assay, and SPR suggested that CPT mitigated renal inflammation and fibrosis by inhibiting the renal STAT3 signaling pathway and downregulating the expression of presenilin-associated rhomboid-like protein (PARL).

The triterpenoids isolated from *C. paliurus* mainly include 3,4-seco-dammarane, dammarane, oleanane, and other types. Dammarane triterpenoids primarily occur as disaccharide glycosides, whereas

3,4-seco-dammarane triterpenoids are mainly monoglycosides, featuring a cleavage between C-3 and C-4. Typically, the C-3 undergoes oxidation to form carboxyl groups (either free or esterified), with double bonds emerging between C-4 and C-23. Consequently, this may lead to distinctive mass spectrometry characteristic ions for dammarane and 3,4-seco-dammarane triterpenoids[23, 30, 31]. Jiang et al. documented that pterocaryoside B produced a fragment ion at *m/z* 371.19 in negative ion mode[40]. Similarly, in this study, mass spectrometry fragment analysis indicated that 3,4-seco-dammarane triterpenoids generated a fragment ion at *m/z* 395.25 in positive ion mode. Consequently, the fragment ion at *m/z* 395.25, retaining the structure of the parent nucleus, could serve as a distinctive fragment ion for 3,4-seco-dammarane triterpenoids, aiding in the identification of components. Derived from the fragment ion and precise molecular weight, nineteen 3,4-seco-dammarane triterpenoids, twelve dammarane triterpenoids, two oleanane triterpenoids, and one nor-dammarane triterpenoid, have been identified in CPT, potentially serving as crucial components for mitigating HN.

Hyperuricemia enhances the expression of inflammatory factors, including IL-1β, TNF-α, and IL-6, which contribute to renal inflammation and fibrosis. Therefore, treating HN requires reducing UA levels and preventing renal injury[11]. The total extract of *C. paliurus* leaves has been shown to lower serum UA and mitigate renal inflammation in hyperuricemia mice, with likely mechanisms involving the suppression of XOD and adenosine deaminase (ADA), modulation of renal urate transporters, and hindrance of the NLRP3/IL-1β signaling pathway[27, 29]. Despite these findings, the therapeutic constituents of the *C. paliurus* leaves for hyperuricemia require further elucidation. Zhu et al. have reported that flavonoid glycosides inhibit XOD activity and inflammation in MSU-induced THP-1 cells[27]. Moreover, the raw polysaccharides derived from the *C. paliurus* leaves have shown XOD inhibitory effects[41]. In the present study, CPT not only curtailed weight loss due to HN but also reduced the levels of PUA, BUN, and UP. Concurrently, CPT alleviated renal fibrosis and lesions, underscored by diminished inflammatory and fibrosis markers. Plasma differential metabolites affected by CPT corresponded with those altered by the aqueous extract of *C. paliurus* leaves[28]. These outcomes indicate that CPT is one of the effective components in C. paliurus leaves for alleviating HN.

Renal excretion of urate is essential for maintaining UA homeostasis. A variety of urate transporters, responsible for both secretion and reabsorption, are located on the renal tubular epithelial cells[3]. Specifically, URAT1 is situated on the apical membrane of these cells and facilitates the reabsorption of urate from the urine back into the cells. Urate is then transferred to the tissue fluid via GLUT9, which is found on the basolateral membrane, ultimately leading to reabsorption into the bloodstream[3]. Uricosuric agents like benzbromarone enhance urate excretion by inhibiting the action of URAT1 and GLUT9, thereby decreasing serum UA levels[17]. OAT1, expressed on the basolateral membrane of renal tubular epithelial cells, mediates the transport of urate into these cells through an exchange with dicarboxylates. Urate is then excreted into the urine via other secretory transporters[1]. Upregulated reabsorption and downregulated secretion transporters both contribute to HN. Modulating urate transporters or inhibiting uric acid production

is an effective strategy for improving purine metabolism[42]. *Cyclocarya paliurus* triterpenoids showed weak XOD inhibition[28]. However, the present study showed that CPT could increase the expression of renal OAT1 and lower the expression of renal URAT1 and GLUT9 to promote urate excretion, indicating that CPT promotes renal urate excretion by enhancing the expression of renal OAT1 and reducing the expression of renal URAT1 and GLUT9 to improve purine metabolism.

Renal fibrosis, marked by the excessive accumulation of extracellular matrix (ECM), emerges as a primary pathological change and mechanism underlying HN, closely associated with serum UA levels[17, 19]. EMT represents an initial critical phase in renal fibrosis, where renal tubular cells lose their epithelial characteristics (evidenced by reduced E-cadherin expression) and transform into mesenchymal phenotype (demonstrated by increased α-SMA and vimentin expression)[22]. STAT3, extensively presented in kidney tissues, orchestrates cell proliferation and differentiation, immune modulation, and inflammatory response. STAT3 can be activated through phosphorylation at Y705 by upstream regulators like IL-6, TGF-β1, and EGFR. Then STAT3 forms heterodimers or homodimers that migrate to the nucleus, directing the transcription of pivotal genes implicated in EMT and renal fibrosis[17, 43]. The expression of Suppressors of cytokine signaling 3 (SOCS3), a negative feedback regulator of STAT3, escalates in response to STAT3 hyperactivation[15, 18, 20, 21]. UA directly triggers the STAT3 pathway in various cells, including HK-2, TCMK-1, and NRK-52E cells, enhancing ECM deposition, EMT, and autophagy[16, 19, 22, 39]. This study leverages network pharmacology and molecular docking, identifying STAT3 as the core target for CPT in mitigating HN. Moreover, CPT attenuates the activation of STAT3 pathways and inhibits EMT in both HN rats and UA-stimulated HK-2 cells. More importantly, both CETSA and SPR results demonstrate that CPT directly binds to STAT3. These insights underscore the potential of CPT to ameliorate HN by targeting STAT3. In contrast to modulating upstream regulators of STAT3, such as JAK2 and MAPK, this study demonstrates that CPT and CYB directly target STAT3 and ameliorate hypertensive nephropathy (HN) by regulating its downstream effector, CSRP2[14-21].

Myofibroblasts are the main cells producing ECM, and the expression of smooth muscle cell (SMC) genes (including actin, cell adhesion molecules, and collagen) is a marker of myofibroblast activation. CSRP2 promotes SMC genes expression via the MRTF/SRF signaling pathway[44]. Additionally, CSRP2 modulates the expression of α-SMA and the activity of SMC genes in cardiomyocytes[45]. CSRP2 exhibits high expression levels in vascular smooth muscle cells and is upregulated during the initial activation phase of hepatic stellate cells through the TGF-β/ALK5/Smad signaling pathway[46]. Moreover, hypoxia suppresses the expression of HLF4 through the TGF-β1/ROCK signaling pathway, thereby increasing CSRP2 expression and exacerbating pulmonary vascular fibrosis. Conversely, CSRP2 knockout has been shown to diminish ECM production[47]. This study indicates that CSRP2 is a downstream gene of STAT3, supported by modulators (S3I-201 and colivelin) and dual-luciferase reporter assays, pending further investigation into its pathophysiological role in HN. PARL is instrumental in regulating the degradation of PINK1 and PGAM5, impacting mitochondrial autophagy that relies on the PINK1/Parkin pathway[48]. The

HN mice induced by a high fructose diet exhibit suppression of PINK/Parkin signaling, leading to mitochondrial autophagy disorders and exacerbating renal fibrosis[49]. S3I-201 exhibited minimal effect on PARL expression in UA-induced HK-2 cells, while CPT significantly inhibited the expression of both CSRP2 and PARL. This suggests that CPT may ameliorate HN by regulating PARL and its associated pathways through other mechanisms, warranting further investigation.

5. Conclusion

In summary, this study demonstrated that CPT mitigated HN through dual hypouricemic and renoprotective effects in an HN rat model. Integrated proteomics, network pharmacology, and experimental validation indicated that CPT alleviated HN by modulating the expression of renal urate transporters and suppressing the STAT3 signaling pathway. This research supports the potential of CPT as a therapeutic agent for HN and hyperuricemia-related diseases.

Acknowledgments

This work was supported by the Hunan Key Research Project (No. 2022SK2031; No. 2020SK2002), Hunan Natural Science Foundation (No.2022JJ30788), Hunan Province Scientific Research Program of Traditional Chinese Medicine (No. C2022041), Major Project of Health Research in Hunan Province (No. W20241006), Furong Laboratory Programs for Science and Technology Development (No. 2023SK2102), Hainan Key Research Project (No. ZDYF2022SHFZ081; No. ZDYF2020213), Central South University College Students Innovation and Entrepreneurship Project (No. YCY2024003; No. CYPY2024001).

Conflict of interest

The authors declare that they have no known competing financial interests or personal relationships that could have appeared to influence the work reported in this paper.

Data Availability

Data will be made available from the corresponding author upon reasonable request.

References

[1] S.L. Yang, H.M. Liu, X.M. Fang, et al., Signaling pathways in uric acid homeostasis and gout: From pathogenesis to therapeutic interventions, Int. Immunopharmacol. 132 (2024) 111932. https://doi.org/10.1016/j.intimp.2024.111932.

[2] C.G. Li, Guideline for the diagnosis and management of hyperuricemia and gout in China (2019), Chin. J. Endocrinol. Metab. 36 (2020) 1-13. https://doi.org/10.3760/cma.j.issn.1000-6699.2020.01.001.

[3] H. Yanai, H. Adachi, M. Hakoshima, et al., Molecular Biological and Clinical Understanding of the Pathophysiology and Treatments of Hyperuricemia and Its Association with Metabolic Syndrome, Cardiovascular Diseases and Chronic Kidney Disease, Int. J. Mol. Sci. 22 (2021) 9221. https://doi.org/10.3390/ijms22179221.

[4] P. Liu, G. Ma, Y. Wang, et al., Therapeutic effects of traditional Chinese medicine on gouty nephropathy: Based on NF-kappaB signaling pathways, Biomed. Pharmacother. 158 (2023) 114199. https://doi.org/10.1016/j.biopha.2022.114199.

[5] X.M. Chen, Practice Guidelines for Diagnosis and Treatment of Hyperuricemia in Kidney Diseases in China (2017), Natl. Med. J. China. 97 (2017) 1927-36. https://doi.org/10.3760/cma.j.issn.0376-2491.2017.25.003.

[6] N. Li, M. Amatjan, P. He, et al., Integration of network pharmacology and intestinal flora to investigate the mechanism of action of Chinese herbal Cichorium intybus formula in attenuating adenine and ethambutol hydrochloride-induced hyperuricemic nephropathy in rats, Pharm. Biol. 60 (2022) 2338-54. https://doi.org/10.1080/13880209.2022.2147551.

[7] M. Zhang, X. Zhu, J. Wu, et al., Prevalence of Hyperuricemia Among Chinese Adults: Findings From Two Nationally Representative Cross-Sectional Surveys in 2015-16 and 2018-19, Front. Immunol. 12 (2021) 791983. https://doi.org/10.3389/fimmu.2021.791983.

[8] F. Butler, A. Alghubayshi, Y. Roman, The Epidemiology and Genetics of Hyperuricemia and Gout across Major Racial Groups: A Literature Review and Population Genetics Secondary Database Analysis, J. Pers. Med. 11 (2021) 231. https://doi.org/10.3390/jpm11030231.

[9] W. Meng, L. Chen, K. Ouyang, et al., Chimonanthus nitens Oliv. leaves flavonoids alleviate hyperuricemia by regulating uric acid metabolism and intestinal homeostasis in mice, Food Sci. Human Wellness 12 (2023) 2440-50. https://doi.org/10.1016/j.fshw.2023.03.011.

[10] Y.Y. Zhu, B.J. Pandya, H.K. Choi, Comorbidities of Gout and Hyperuricemia in the US General Population: NHANES 2007-2008, Am. J. Med. 125 (2012) 679-87. https://doi.org/10.1016/j.amjmed.2011.09.033.

[11] L. Yang, B. Wang, L. Ma, et al., Traditional Chinese herbs and natural products in hyperuricemia-induced chronic kidney disease, Front. Pharmacol. 13 (2022) 971032. https://doi.org/10.3389/fphar.2022.971032.

[12] G.Y. Tang, S. Li, Y. Xu, et al., Renal herb formula protects against hyperuricemic nephropathy by inhibiting apoptosis and inflammation, Phytomedicine 116 (2023) 154812. https://doi.org/10.1016/j.phymed.2023.154812.

[13] J. Pan, M. Shi, F. Guo, et al., Pharmacologic inhibiting STAT3 delays the progression of kidney fibrosis in hyperuricemia-induced chronic kidney disease, Life Sci. 285 (2021) 119946. https://doi.org/10.1016/j.lfs.2021.119946.

[14] M.X. Lu, J.Y. Yin, T.S. Xu, et al., Fuling-Zexie formula attenuates hyperuricemia-induced nephropathy and inhibits JAK2/STAT3 signaling and NLRP3 inflammasome activation in mice, J. Ethnopharmacol. 319 (2023) 117262. https://doi.org/10.1016/j.jep.2023.117262.

[15] Y.Y. Zhang, S. Wang, X. Dai, et al., Simiao San alleviates hyperuricemia and kidney inflammation by inhibiting NLRP3 inflammasome and JAK2/STAT3 signaling in hyperuricemia mice, J. Ethnopharmacol. 312 (2023) 116530. https://doi.org/10.1016/j.jep.2023.116530.

[16] J. Wang, X.W. Bu, X.P. Qiu, et al., Qinling liquid ameliorates renal immune inflammatory damage via activating autophagy through AMPK/Stat3 pathway in uric acid nephropathy, Cytokine 163 (2023) 156120. https://doi.org/10.1016/j.cyto.2022.156120.

[17] L.R. Sun, Q. Liu, Y.B. Zhang, et al., Fucoidan from Saccharina japonica Alleviates Hyperuricemia-Induced Renal Fibrosis through Inhibiting the JAK2/STAT3 Signaling Pathway, J. Agric. Food Chem. 71 (2023) 11454-65. https://doi.org/10.1021/acs.jafc.3c01349.

[18] T. Liu, H. Gao, Y. Zhang, et al., Apigenin Ameliorates Hyperuricemia and Renal Injury through Regulation of Uric Acid Metabolism and JAK2/STAT3 Signaling Pathway, Pharmaceuticals (Basel) 15 (2022) https://doi.org/10.3390/ph15111442.

[19] Q. Ren, S. Tao, F. Guo, et al., Natural flavonol fisetin attenuated hyperuricemic nephropathy via inhibiting IL-6/JAK2/STAT3 and TGF-beta/SMAD3 signaling, Phytomedicine 87 (2021) 153552. https://doi.org/10.1016/j.phymed.2021.153552.

[20] M. Wang, J. Zhao, N. Zhang, et al., Astilbin improves potassium oxonate-induced hyperuricemia and kidney injury through regulating oxidative stress and inflammation response in mice, Biomed. Pharmacother. 83 (2016) 975-88. https://doi.org/10.1016/j.biopha.2016.07.025.

[21] G. Lin, Q. Yu, L. Xu, et al., Berberrubine attenuates potassium oxonate- and hypoxanthine-induced hyperuricemia by regulating urate transporters and JAK2/STAT3 signaling pathway, Eur. J. Pharmacol. 912 (2021) 174592. https://doi.org/10.1016/j.ejphar.2021.174592.

[22] S.H. Wu, M.X. Yan, J.Y. Liu, et al., Clerodendranthus spicatus inhibits epithelial-mesenchymal transition of renal tubular cells through the NF-κB/Snail signalling pathway in hyperuricaemia nephropathy, Pharm. Biol. 61 (2023) 1274-85. https://doi.org/10.1080/13880209.2023.2243086.

[23] Z. Chen, Y. Jian, Q. Wu, et al., Cyclocarya paliurus (Batalin) Iljinskaja: Botany, Ethnopharmacology, phytochemistry and pharmacology, J. Ethnopharmacol. 285 (2022) 114912. https://doi.org/10.1016/j.jep.2021.114912.

[24] J. Zhao, Z. Wang, D. Xu, et al., Advances on Cyclocarya paliurus polyphenols: Extraction, structures, bioactivities and future perspectives, Food Chem 396 (2022) 133667. https://doi.org/10.1016/j.foodchem.2022.133667.

[25] G. Wang, W. Zhang, K. Cheng, et al., Effects of Penicillium EF-2 fermentation on Cyclocarya paliurus polysaccharide and preliminary mechanism exploration: Physicochemical, characterisation, in vitro immunomodulatory activity, Food Bioscience 63 (2025) https://doi.org/10.1016/j.fbio.2024.105777.

[26] H. Xi, W. Xu, F. He, et al., Spatial metabolome of biosynthesis and metabolism in Cyclocarya paliurus leaves, Food Chemistry 443 (2024) https://doi.org/10.1016/j.foodchem.2024.138519.

[27] L.-H. Zhu, Y.-Y. Xu, L.-p. Zhu, et al., Protective effects of Cyclocarya paliurus on hyperuricemia and urate-induced inflammation, J. Funct. Food. 94 (2022) https://doi.org/10.1016/j.jff.2022.105130.

[28] R. Gui, Y.K. Wang, J.P. Wu, et al., Cyclocarya paliurus leaves alleviate hyperuricemic nephropathy via modulation of purine metabolism, antiinflammation, and antifibrosis, J. Funct. Food. 103 (2023) 105485. https://doi.org/10.1016/j.jff.2023.105485.

[29] D. Luo, D. Chen, X.C. Bai, et al., Effects of Selenium-enriched Cyclocarya paliurus and Polygonatum sibiricum Compounds on Lowering Uric Acid in Mice with Hyperuricemia, Pharmacy Today 31 (2021) 909-17. https://doi.org/10.12048/j.issn.1674-229X.2021.12.006.

[30] Y.M. Shao, T.T. Li, C.E. Wu, et al., A Review on Extraction and Biological Activities of Triterpenoid from Cyclocarya paliurus, Food Rev. Int. 40 (2023) 1374-94. https://doi.org/10.1080/87559129.2023.2213307.

[31] S.R. Zhang, J.Y. He, J. Li, et al., Triterpenoid Compounds from Cyclocarya paliurus: A Review of Their Phytochemistry, Quality Control, Pharmacology, and Structure–Activity Relationship, Am. J. Chin. Med. 51 (2023) 1-35. https://doi.org/10.1142/S0192415X2350088X.

[32] J. Li, J.Y. He, H.B. He, et al., Sweet triterpenoid glycoside from Cyclocarya paliurus ameliorates obesity-induced insulin resistance through inhibiting the TLR4/NF-κB/NLRP3 inflammatory pathway, Curr. Res. Food Sci. 8 (2024) 100677. https://doi.org/10.1016/j.crfs.2024.100677.

[33] R. Yang, S. Xu, X. Zhang, et al., Cyclocarya paliurus triterpenoids attenuate glomerular endothelial injury in the diabetic rats via ROCK pathway, J. Ethnopharmacol. 291 (2022) 115127. https://doi.org/10.1016/j.jep.2022.115127.

[34] X.X. Zhang, C.H. Jiang, Y. Liu, et al., Cyclocarya paliurus triterpenic acids fraction attenuates kidney injury via AMPK-mTOR-regulated autophagy pathway in diabetic rats, Phytomedicine 64 (2019) 153060. https://doi.org/10.1016/j.phymed.2019.153060.

[35] X. Zheng, M.G. Zhao, C.H. Jiang, et al., Triterpenic acids-enriched fraction from Cyclocarya paliurus attenuates insulin resistance and hepatic steatosis via PI3K/Akt/GSK3β pathway, Phytomedicine 66 (2019) 153130. https://doi.org/10.1016/j.phymed.2019.153130.

[36] C. Jiang, Y. Wang, Q. Jin, et al., Cyclocarya paliurus Triterpenoids Improve Diabetes-Induced Hepatic Inflammation via the Rho-Kinase-Dependent Pathway, Front. Pharmacol. 10 (2019) 811. https://doi.org/10.3389/fphar.2019.00811.

[37] Q. Li, P. Liu, C. Wu, et al., Integrating network pharmacology and pharmacological validation to explore the effect of Shi Wei Ru Xiang powder on suppressing hyperuricemia, Journal of Ethnopharmacology 298 (2022) https://doi.org/10.1016/j.jep.2022.115679.

[38] H. Liu, Z. Chen, M. Liu, et al., The Terminalia chebula Retz extract treats hyperuricemic nephropathy by inhibiting TLR4/MyD88/NF-κB axis, Journal of Ethnopharmacology 322 (2024) https://doi.org/10.1016/j.jep.2023.117678.

[39] H.L. Li, X.J. Liu, M.H. Lee, et al., Vitamin C alleviates hyperuricemia nephropathy by reducing inflammation and fibrosis, J. Food Sci. 86 (2021) 3265-76. https://doi.org/10.1111/1750-3841.15803.

[40] C. Jiang, Q. Wang, Y. Wei, et al., Cholesterol-lowering effects and potential mechanisms of different polar extracts from Cyclocarya paliurus leave in hyperlipidemic mice, J. Ethnopharmacol. 176 (2015) 17-26. https://doi.org/10.1016/j.jep.2015.10.006.

[41] H.X. Su, G. Jing, M. Jiang, et al., Optimization of preparation technology for crude polysaccharide CP50 from Cyclocarya paliurus and its inhibitory effects on xanthine oxidase, Food and Fermentation Industries 49 (2023) 88-93. https://doi.org/10.13995/j.cnki.11-1802/ts.033408.

[42] Y. Lu, X.-X. Fan, S.-L. Zhao, et al., Supplements extracted from Lophatherum gracile Brongn. ameliorates hyperuricemia by regulating nucleotide metabolic enzymes and urate transporters, Food & Medicine Homology 3 (2025) 9420099. https://doi.org/10.26599/fmh.2026.9420099.

[43] J.T. Yu, S. Fan, X.Y. Li, et al., Novel insights into STAT3 in renal diseases, Biomed. Pharmacother. 165 (2023) 115166. https://doi.org/10.1016/j.biopha.2023.115166.

[44] K. Hayashi, S. Horoiwa, K. Mori, et al., Role of CRP2-MRTF interaction in functions of myofibroblasts, Cell Struct. Funct. 48 (2023) 83-98. https://doi.org/10.1247/csf.23004.

[45] D.F. Chang, N.S. Belaguli, J. Chang, et al., LIM-only protein, CRP2, switched on smooth muscle gene activity in adult cardiac myocytes, Proc. Natl. Acad. Sci. U. S. A. 104 (2007) 157-62. https://doi.org/10.1073/pnas.0605635103.

[46] J. Herrmann, E. Borkham Kamphorst, U. Haas, et al., The expression of CSRP2 encoding the LIM domain protein CRP2 is mediated by TGF-beta in smooth muscle and hepatic stellate cells, Biochem. Biophys. Res. Commun. 345 (2006) 1526-35. https://doi.org/10.1016/j.bbrc.2006.05.076.

[47] X. Chen, X. Wei, S. Ma, et al., Cysteine and glycine rich protein 2 exacerbates vascular fibrosis in pulmonary hypertension through the nuclear translocation of yes-associated protein and transcriptional coactivator with PDZ-binding motif, Toxicol. Appl. Pharmacol. 457 (2022) 116319. https://doi.org/10.1016/j.taap.2022.116319.

[48] E. Polachova, K. Bach, E. Heuten, et al., Chemical Blockage of the Mitochondrial Rhomboid Protease PARL by Novel Ketoamide Inhibitors Reveals Its Role in PINK1/Parkin-Dependent Mitophagy, J. Med. Chem. 66 (2023) 251-65. https://doi.org/10.1021/acs.jmedchem.2c01092.

[49] C. Zhang, Y. Song, L. Chen, et al., Urolithin A Attenuates Hyperuricemic Nephropathy in Fructose-Fed Mice by Impairing STING-NLRP3 Axis-Mediated Inflammatory Response via Restoration of Parkin-Dependent Mitophagy, Front. Pharmacol. 13 (2022) 907209. https://doi.org/10.3389/fphar.2022.907209.